

# Spatial mode effects in a cavity EIT-based quantum memory with ion Coulomb crystals

Kasper R. Zangenberg, Aurélien Dantan, Michael Drewsen

QUANTOP, Danish National Research Foundation Center for Quantum Optics,  
Department of Physics and Astronomy, Aarhus University, DK-8000 Århus C.,  
Denmark

**Abstract.** Quantum storage and retrieval of light in ion Coulomb crystals using cavity electromagnetically induced transparency is investigated theoretically. It is found that, when both the control and probe fields are coupled to the same cavity mode, their transverse mode profile affects the quantum memory efficiency in a non-trivial way. Under such conditions the control field parameters and crystal dimensions that maximize the memory efficiency are calculated.

PACS numbers: 42.50.Gy, 42.50.Ex, 42.50.Pq

Submitted to: *J. Phys. B: At. Mol. Phys.*

## 1. Introduction

Motivated by applications in the field of quantum information processing [1, 2, 3, 4], quantum memory devices are being investigated in a variety of physical systems and with different techniques and protocols (for a review see e.g. [5, 6]). Among the various criteria used to evaluate the performance of a quantum memory, are generally of interest its fidelity, its efficiency, its storage time and its multimode capacity [5]. For optical quantum memories, in which an input light pulse is stored into a material system and subsequently retrieved, the efficiency can simply be defined as the ratio between the energies of the output and input pulses. For an important class of optical quantum memories based on electromagnetically induced transparency (EIT) processes in atomic ensembles [7, 8, 9, 10, 11, 12, 13, 14, 15], the efficiency crucially depends on the optical depth of the ensemble [5]. Enclosing the atomic medium in an optical cavity allows for substantially increasing the effective optical depth experienced by the light and cavity EIT protocols have been proposed to achieve high storage efficiencies [16, 17, 18, 19, 20].

Among the variety of atomic systems studied in connection with quantum memories, an ion Coulomb crystals positioned in an optical cavity has been suggested as a good candidate to realize a high-performance quantum memory, potentially meeting the criteria mentioned above [21]. Recently, this analysis has been backed up by a series of

key experimental results. Substantial effective optical depths can indeed be realized by strongly coupling large ion Coulomb crystals to a cavity field and long coherence times can be achieved in such a system [22, 23]. Furthermore, strong coupling to various spatial cavity modes has been demonstrated [24], which is promising for multimode storage. Finally, cavity EIT has recently been observed with ion Coulomb crystals using an *all-cavity* geometry in which both the probe and control fields are coupled to the same cavity mode [25].

In this specific cavity EIT geometry, it has been observed, both theoretically [26] and experimentally [25], that the spatial transverse profile of the control field has a significant effect on the probe transmission/reflection lineshapes and dynamics. This is in contrast with more standard cavity EIT configurations in which the control field is free-propagating and has typically a much larger extension than the probe field [27, 28, 29, 30, 31, 32, 33]. Since the all-cavity geometry is one natural realization of the scheme presented in [21], it is interesting to investigate its implications for the performance of such an ion Coulomb crystal-based quantum memory. In this paper, we extend the existing theoretical models for cavity EIT-based light storage and retrieval [16, 17, 18, 19, 20] to the all-cavity configuration and numerically investigate the effect of the transverse mode profile of the fields on the quantum memory efficiency. We find in particular that the optimal efficiency depends not only on the cooperativity parameter, but also on the radial extension of the crystal, as a result of the more complex spatial mode structure defined by the fields inside the atomic medium. Using parameters taken from current experiments with ion Coulomb crystals [22, 25], our simulations predict that similarly high-efficiencies ( $> 90\%$ ) should however be obtainable in the all-cavity configuration.

The paper is structured as follows: in sec. 2 the theoretical model for the light storage and retrieval is presented, starting with a general description in secs. 2.1 and 2.2, an optimization of the quantum memory efficiency in the standard configuration for smoothly-varying single-photon input pulses, following the approach of ref. [20], in sec. 2.3 and the “cylindrical shell” model used for the simulations of the all-cavity configuration in sec. 2.4. Section 3 presents the results of the numerical simulations based on typical experimental parameters for ion Coulomb crystals (sec. 3.1) and for light fields coupled to the cavity fundamental  $\text{TEM}_{00}$  mode (sec. 3.2) and a higher-order Laguerre-Gauss  $\text{LG}_{01}$  mode (sec. 3.3). A brief conclusion on the implications of these results for experiments are given in sec. 4.

## 2. Theoretical model

### 2.1. Description of the model

Inspired by the experiments of [25] we base our description of the light-matter interaction on the model developed in [26]. We consider an ensemble of three-level  $\Lambda$  atoms with two ground states,  $|1\rangle$  and  $|2\rangle$ , and an excited state  $|3\rangle$ . The atoms interact with a cavity

probe field on the  $|1\rangle \rightarrow |3\rangle$  transition and a classical control field  $\Omega$  on the  $|2\rangle \rightarrow |3\rangle$  transition. Both fields are assumed to be resonant with the atomic transitions and the cavity is tuned to resonance with the probe field. Since we are mostly interested in discussing the effects of the transverse mode profile of the fields, we neglect the longitudinal variation of the atom-field couplings. This goes for atoms in a running-wave cavity [29, 32, 34], but can also apply to a standing-wave cavity geometry for atoms with either well-defined positions with respect to the cavity standing-wave [28, 35, 36] or atoms whose motion average out the longitudinal standing-wave structure of the fields over the relevant timescales [25, 26]. The atomic ensemble extension is also assumed to be much smaller than the cavity field Rayleigh range. The cavity is furthermore taken to be single-ended and with lossless mirrors (fig. 1).

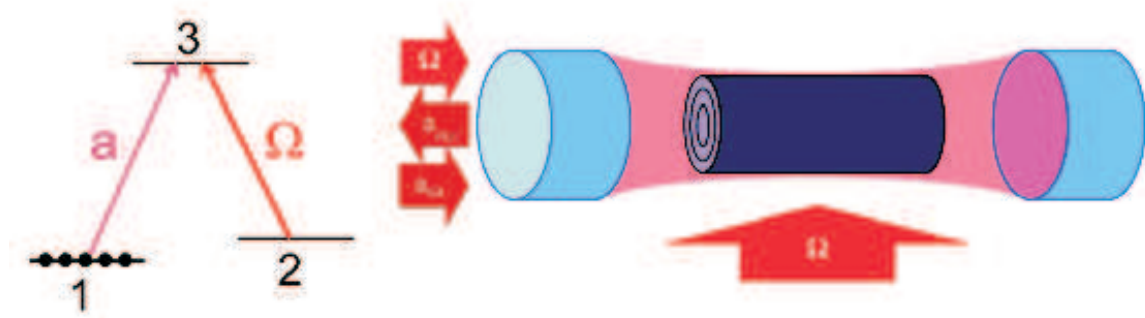


**Figure 1.** (Color online) Left: Three-level  $\Lambda$  atomic structure considered. Right: a cylindrically symmetric atomic medium, composed of  $\Lambda$  atoms, is enclosed in a single-ended optical cavity where it interacts with a probe field and a control field in an EIT situation. Two configurations are investigated: one in which both fields are coupled to the same cavity mode - and have therefore the same waist, and one in which the control field has a constant intensity profile over the ensemble.

We will also assume that the fields injected into the cavity are *smooth* pulses whose envelopes are slowly varying with respect to the cavity field and atomic decay rates, in the sense of [20]. For the light storage and retrieval dynamics we will follow the approach of refs. [16, 19, 20] and assume a standard write-store-read temporal sequence. During the write phase the input probe field is injected into the cavity and the control field is adiabatically turned off to ensure *temporal impedance matching* [18]. Both fields are turned off during the store phase, and the control field is adiabatically turned back on during the readout, causing the emission of an output probe pulse.

Denoting by  $\hat{\sigma}_{\mu\nu}^{(k)} = |\mu\rangle\langle\nu|_k$  the individual atomic operator for the  $k$ -th atom positioned at  $\mathbf{r}_k$  and by  $\hat{a}$  the annihilation operator for the intracavity probe field, the interaction Hamiltonian in the rotating wave approximation and the rotating frame reads

$$H = -\hbar g \sum_k \Psi_p(r_k) \hat{\sigma}_{31}^{(k)} \hat{a} - \hbar \Omega(t) \sum_k \Psi_c(r_k) \hat{\sigma}_{32}^{(k)} + \text{h.c.} \quad (1)$$

where  $g$  is the single-atom maximal coupling rate (at the center of the cavity mode),

$\Psi_{p,c}(r)$  are the probe and control field transverse mode profiles (with the longitudinal dependence neglected) and  $\Omega(t)$  the time-varying Rabi frequency of the control field.

## 2.2. Equations of motion in EIT

We consider a typical EIT regime in which all the atoms are initially in level  $|1\rangle$  and in which the control field is much more intense than the probe field, assumed to be at the single-photon level. One can then assume that almost all the atoms stay in  $|1\rangle$  at all times and perform a standard first-order treatment in the probe field [2]. The Heisenberg equations of motion for the relevant operators, namely the intracavity probe field  $\hat{a}$ , the atomic optical coherences  $\hat{\sigma}_{13}^{(k)}$  and the atomic ground state coherences  $\hat{\sigma}_{12}^{(k)}$ , are given by

$$\dot{\hat{a}} = -\kappa\hat{a} + ig \sum_k \Psi_p(r_k) \hat{\sigma}_{13}^{(k)} + \sqrt{2\kappa}\hat{a}_{in}, \quad (2)$$

$$\dot{\hat{\sigma}}_{13}^{(k)} = -\gamma\hat{\sigma}_{13}^{(k)} + ig\Psi_p(r_k)\hat{a} + i\Omega(t)\Psi_c(r_k)\hat{\sigma}_{12}^{(k)} + \hat{F}_{13}^{(k)}, \quad (3)$$

$$\dot{\hat{\sigma}}_{12}^{(k)} = -\gamma_0\hat{\sigma}_{12}^{(k)} + i\Omega^*(t)\Psi_c(r_k)\hat{\sigma}_{13}^{(k)} + \hat{F}_{13}^{(k)}, \quad (4)$$

and the input-output relation

$$\hat{a}_{out} = \sqrt{2\kappa}\hat{a} - \hat{a}_{in}, \quad (5)$$

where  $\kappa$  is the cavity field decay rate,  $\hat{a}_{in}$  and  $\hat{a}_{out}$  are the annihilation operators associated with the input and output probe fields, respectively.  $\gamma$  and  $\gamma_0$  are the atomic dipole and ground state coherence decay rates, respectively, and  $\hat{F}_{13}^{(k)}$  and  $\hat{F}_{12}^{(k)}$  the corresponding Langevin noise operators.

Following ref. [20], we assume a single-photon input and calculate the quantum memory efficiency by first solving in time the semiclassical counterparts of (2)-(5) for given input probe and control field pulses

$$\dot{a} = -\kappa a + ig \sum_k \Psi_p(r_k) \sigma_{13}^{(k)} + \sqrt{2\kappa}a_{in}, \quad (6)$$

$$\dot{\sigma}_{13}^{(k)} = -\gamma\sigma_{13}^{(k)} + ig\Psi_p(r_k)a + i\Omega(t)\Psi_c(r_k)\sigma_{12}^{(k)}, \quad (7)$$

$$\dot{\sigma}_{12}^{(k)} = -\gamma_0\sigma_{12}^{(k)} + i\Omega^*(t)\Psi_c(r_k)\sigma_{13}^{(k)}, \quad (8)$$

$$a_{out} = \sqrt{2\kappa}a - a_{in}, \quad (9)$$

and, secondly, by computing

$$\eta_{tot} \equiv \frac{\int_r |a_{out}(t)|^2 dt}{\int_w |a_{in}(t)|^2 dt}, \quad (10)$$

where the subscripts  $w$  and  $r$  refer to a summation over the whole duration of the write and read process, respectively.  $\eta_{tot}$  then represents the ratio of the number of retrieved photons to the number of incoming photons, and provides a good measure of the quality of the mapping (for other measures see e.g. [5, 6]). To simplify the discussion we will in the following neglect the decay of the ground state coherence during the whole process and set  $\gamma_0 = 0$ . The duration of the storage phase is then simply chosen such that the dynamics of the write and read phases occur in well-separated time windows.

### 2.3. Efficiency optimization in the case of an extended control field

If the waist of the control field is much larger than the probe field, as in many EIT experiments, one can neglect the transverse variations of the control field intensity over the section of the atomic ensemble that interacts with the probe field. Following, e.g. [26], one can define an effective number of atoms interacting with the probe field

$$N = \sum_k \Psi_p(r_k)^2 \quad (11)$$

and collective operators for the ground state coherence and the optical dipole by

$$\hat{S} = \frac{1}{\sqrt{N}} \sum_k \Psi_p(r_k) \hat{\sigma}_{12}^{(k)}, \quad \hat{P} = \frac{1}{\sqrt{N}} \sum_k \Psi_p(r_k) \hat{\sigma}_{13}^{(k)}. \quad (12)$$

Equations (6)-(9) can be straightforwardly rewritten as

$$\dot{a} = -\kappa a + i g_N P + \sqrt{2\kappa} a_{in}, \quad (13)$$

$$\dot{P} = -\gamma P + i g_N a + i \Omega(t) S, \quad (14)$$

$$\dot{S} = i \Omega^*(t) P, \quad (15)$$

$$a_{out} = \sqrt{2\kappa} a - a_{in}, \quad (16)$$

where  $g_N = g\sqrt{N}$  is the collectively enhanced coupling rate [2].

In this collective mode picture, the input photonic state is mapped during the write phase onto a collective spin-wave described by  $S$  and one can define a *write* efficiency by taking the ratio of the number of atomic excitations and the number of input photons,

$$\eta_w = \frac{|S(T_w)|^2}{\int_w |a_{in}(t)|^2 dt}, \quad (17)$$

where  $T_w$  is the end time of the write phase [20]. Similarly, one can define a readout efficiency by the ratio of the number of output photons and the number of atomic excitations before readout

$$\eta_r = \frac{\int_w |a_{out}(t)|^2 dt}{|S(T_r)|^2}, \quad (18)$$

where  $T_r$  is the start time of the read phase. In the adiabatic limit, i.e. for input pulses with duration  $T$  such that  $2TC\gamma \gg 1$ , one can derive the optimal control pulse that maximizes the read and write efficiencies, which can be shown to scale as [19, 20]

$$\eta_{w,r}^{opt} = \frac{2C}{1 + 2C}, \quad (19)$$

where

$$C = \frac{g^2 N}{2\kappa\gamma} \quad (20)$$

is the cooperativity parameter  $\ddagger$ . In absence of decoherence during the storage phase, the optimal total efficiency thus scales as

$$\eta_{tot}^{opt} = \left( \frac{2C}{1 + 2C} \right)^2, \quad (21)$$

$\ddagger$  Note the factor 2 difference with respect to [20].

and increases with the effective number of atoms defined by the spatial overlap of the ensemble and the probe field [Eq. (11)].

#### 2.4. Effect of the control field's transverse profile

If the waist of the control field  $w_c$  is no longer very large, but comparable to that of the probe field  $w_p$  – as it will be the case in an all-cavity geometry for instance [25, 26] – the previous results no longer apply, and one must evaluate the effect of the control field transverse profile on the storage and retrieval efficiencies. With the approximations made in Sec. 2.2 and having specifically in mind ion Coulomb crystals as the physical storage medium, we assimilate the atomic ensemble to a cylinder with length  $L$  and radius  $R$  (fig. 1), and slice it into  $n$  cylindrical shells of thickness  $d \ll w_p, w_c$  ( $R = nd$ ). We also assume that  $d$  is much larger than the mean interparticle distance. Although it is not essential, we take the atomic density  $\rho$  to be constant throughout the ensemble, which is the case for large ion Coulomb crystals in linear Paul traps [37], and we consider cavity modes with cylindrical symmetry. We proceed by defining collective operators for the  $j$ th-slice as

$$\hat{P}_j = \sigma n_j \hat{\sigma}_{13}^{(j)}, \quad \hat{S}_j = \sigma n_j \hat{\sigma}_{12}^{(j)}, \quad (22)$$

where the subscript  $j$  refers to an atom in the  $j$ -th slice with position  $r_j = d(j - 1/2)$  ( $j = 1..n$ ) and where  $\sigma = \rho L$  is the atomic cross-sectional density. The corresponding semiclassical equations of motion are then

$$\dot{a} = -\kappa a + ig \sum_{j=1}^n \Psi_p(r_j) P_j + \sqrt{2\kappa} a_{in}, \quad (23)$$

$$\dot{P}_j = -\gamma P_j + ig \sigma n_j \Psi_p(r_j) a + i\Omega(t) \Psi_c(r_j) S_j, \quad (24)$$

$$\dot{S}_j = i\Omega^*(t) \Psi_c(r_j) S_j, \quad (25)$$

where the modefunctions  $\Psi_{p,c}$  are evaluated at  $r_j$ .

It is clear from eqs. (23),(24),(25) that, unless  $|\Psi_c(r_j)| = 1$  like in the previous section, it is no longer possible to define collective spatial eigenmodes of the problem that would yield closed equations of the form (13),(14),(15). In particular, these equations show that adjacent shells are coupled together by the control field. The spatial mapping of the probe field onto the ground state spin now depends on the control field transverse profile, in addition to that of the probe field. Because of the intershell coupling during the mapping the radial extension of the ensemble now becomes a parameter which affects the memory efficiency in a non-trivial way.

In the following section we numerically solve these equations of motion for a fixed probe field pulse basing ourselves on the analytical control field pulse derived from the temporal optimization of sec. 2.3 in absence of effects due to the control field transverse profile. Note that, because of the impossibility of defining analytically a spatial collective spin-mode during the write or read phase, and thereby of defining write or read efficiencies, this optimization is performed numerically using the total efficiency  $\eta_{tot}$  as a figure of merit.

### 3. Numerical results

#### 3.1. Physical system considered and input parameters

To solve the problem of optimizing the quantum memory efficiency in the conditions of the previous section we take for the physical storage medium an ion Coulomb crystal, trapped and laser-cooled in a linear Paul trap, with the optical cavity positioned along the trap axis, as in [22, 24, 23, 25]. Although single-component ion Coulomb crystals (i.e. consisting of only ion species) have spheroidal shape and may therefore deviate from the cylindrical shell model (unless they are sufficiently prolate), the inner component of a prolate two-species crystal can be assimilated to a good approximation to a uniform density cylinder [37, 38]. We consider the cavity EIT configuration used in [25], in which both the control and probe fields are frequency degenerate and orthogonally polarized in order to create EIT between Zeeman sub-states of the  $3d\ ^3D_{3/2}$  sub-level of  $^{40}\text{Ca}^+$ . In these experiments both fields are coupled resonantly or near-resonantly to the same cavity mode ( $\text{TEM}_{00}$ ). We thus take Gaussian transverse profiles  $\Psi_{p,c}(r) = \exp(-r^2/w_{p,c}^2)$ , and compare the extended control field configuration ( $w_c \rightarrow \infty$ ) and the finite control field waist configuration ( $w_c = w_p$ ).

For the 11.8 mm-long, close to confocal cavity of [25] with an incoupling mirror transmission of 1500 ppm and an interaction on the  $3d\ ^3D_{3/2}, m_J = +3/2 \rightarrow 4p\ ^2P_{1/2}, m_J = +1/2$  (probe) and  $3d\ ^3D_{3/2}, m_J = -1/2 \rightarrow 4p\ ^2P_{1/2}, m_J = +1/2$  (control) transitions, one finds  $(g, \kappa, \gamma) = 2\pi \times (0.37, 1.5, 11.3)$  MHz §. With a radius of curvature of 10 mm, the waist of the probe field at the center of the cavity is  $w_p = 37\ \mu\text{m}$ . For crystals with typical length of a few mm and radius of up to a few hundreds of microns, neglecting the longitudinal curvature of the fields over the crystal modevolume is well-justified [22, 24].

For the sake of the discussion, we assume for the probe field a hyperbolic secant input pulse of the form

$$a_{in}(t) = \frac{1}{\sqrt{T}} \text{sech}(2t/T), \quad (26)$$

where  $T$  is the probe pulse duration ||. In the adiabatic limit ( $TC\gamma \gg 1$ ) considered previously in sec. 2.3 and the extended control field configuration ( $w_c \rightarrow \infty$ ), the control field pulses which optimize the write and read efficiencies are given by [20]

$$\Omega_w(t) = A \sqrt{\frac{2\gamma(1+2C)}{T}} \frac{1}{\sqrt{1 + \exp(4t/T)}} \quad (27)$$

for the write phase, and its time-reversed counterpart

$$\Omega_r(t) = \Omega_w(-t + T_r + T_s), \quad (28)$$

§ Note that, in constrast to [22, 25], the single-ion coupling rate has been scaled by a factor  $1/\sqrt{2}$  to account for the longitudinal averaging over the standing-wave structure.

|| This form for the probe pulse is taken for convenience, as one gets an analytical expression for the optimal control field pulse [16], but the numerical simulations show that the exact form of the input pulse is not critical.

for the readout phase. In the extended configuration the prefactor  $A$  is equal to unity. As we will see in the next section, the previous control field temporal profiles are still found to be optimal with respect to maximizing the efficiency in the finite waist configuration, the main difference being in the optimal control field amplitude scaling factor  $A$ .

### 3.2. Results for the $TEM_{00}$ mode

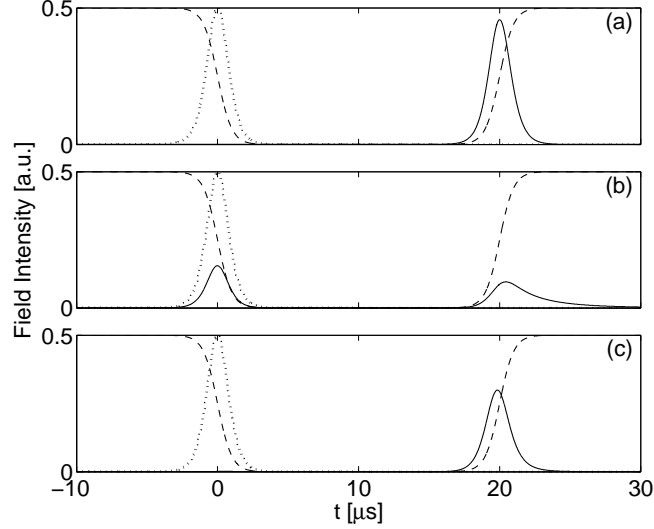


**Figure 2.** Temporal storage and retrieval sequence for (a) an extended control field ( $w_c \rightarrow \infty$ ), (b) a control field with finite waist ( $w_c = w_p$ ) and non-optimized amplitude ( $A = 1$ ) and (c) a control field with finite waist ( $w_c = w_p$ ) and optimized amplitude ( $A = 2.45$ ). The dotted and solid curves are the normalized input and output field intensities,  $|a_{in}(t)|^2$  and  $|a_{out}(t)|^2$ , respectively. The dashed curve shows the control field intensity  $\Omega(t)^2$ , scaled such that its maximum value is 0.5.  $T_r = T_w = 10 \mu s$ . See text for the value of the other parameters.

Figure 2a shows the results of a storage and retrieval sequence for a crystal with density  $\rho = 6.1 \times 10^8 \text{ cm}^{-3}$ , length  $L = 3 \text{ mm}$  and radius  $R = 100 \mu m$ , an input probe pulse of the form (26) with duration  $T = 2 \mu s$  and an extended control field of the form (27),(28) with  $A = 1$ . For such a large crystal ( $R \gg w_c$ ), the effective number of ions as defined by (11) is  $N = 3936$ , yielding a cooperativity parameter  $C \simeq 16.7$ . The write and read efficiencies are found to be  $\eta_w = 0.970$  and  $\eta_r = 0.971$ , respectively, close to the theoretical value of  $\eta_{r,w}^{opt} = 0.971$ , and yielding a total efficiency  $\eta_{tot} = 0.942$  ( $\eta_{tot}^{opt} = 0.943$ ). Figure 2b shows the results of the same sequence and parameters for a control field with  $w_c = w_p$ . It is clear that, during the write phase, perfect temporal impedance matching is not achieved, as a substantial amount of the incoming light is reflected. This is in itself not surprising as the prefactor  $A = 1$  is only optimal in the extended configuration, and one expects that, in the finite waist configuration, the ions see on average a control field with lower Rabi frequency. As can be seen from fig. 2c, close to perfect impedance matching can be recovered by increasing the control field amplitude ( $A \simeq 2.45$ ). The total efficiency  $\eta_{tot} = 0.667$  remains, however, lower



than in the corresponding extended configuration. We checked numerically that varying the control field pulse switching time and shape, or having different amplitudes/time evolutions profiles during write and read, does not increase the efficiency. We also checked that these results do not significantly depend on  $T$  as long as one stays in the adiabatic limit.

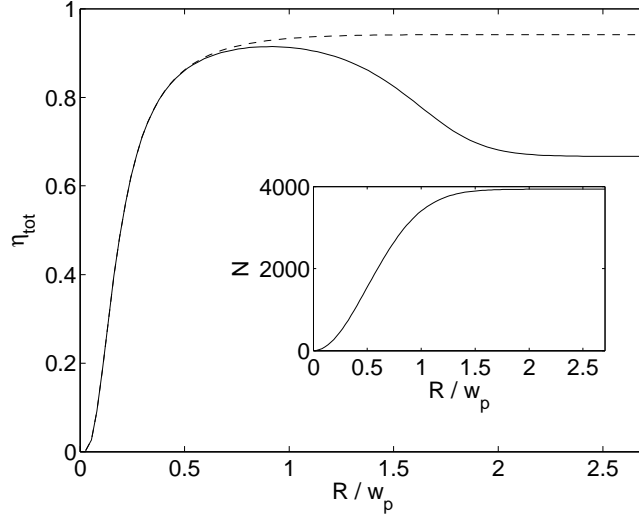


**Figure 3.** Variation of the total efficiency  $\eta_{tot}$  as a function of the crystal radius  $R$ , for the same parameters as in fig. 2. The dashed line shows the extended control field case while the solid line shows the finite waist case for which the control field amplitude has been optimized for each radius. The inset shows the variation of the effective number of ions [eq. (11)] as a function of the crystal radius  $R$ .

The lack of critical dependence of the optimal efficiency with respect to the temporal parameters found in the simulations seems to indicate, in agreement with the analysis of sec. 2.4, that the spatial profile of the control field now plays a significant role in the mapping process. To investigate this effect further we show in fig. 3 the variation of the effective number of ions and the (temporally) optimized efficiency as a function of the crystal radius in the two configurations. The other parameters are kept the same as previously. While in the extended control field configuration the efficiency increases, together with  $N$ , with the crystal radius and saturates when  $R \gg w_p$ , it reaches a maximum for  $R \sim w_p$  in the finite waist configuration, before decreasing and reaching a constant level at high radius. The total efficiency peaks at  $R \simeq 0.95w_p$  with a value of 0.914 ( $A = 1.5$ ), closer to the theoretical value of  $\eta_{tot}^{opt} = 0.932$  (for this radius  $N = 3279$  and  $C = 13.9$ ). The decrease for  $R > w_p$  radius may appear surprising, since more ions are being added to the crystal and one could expect an enhanced efficiency due to the stronger coupling to the probe field. However, for a finite waist control field, the spatial spin mode defined during writing – or, for that matter, during reading – is no longer that of the probe, but depends on the overlap of both the probe *and* the control field transverse profiles in the crystal. As the radius of the crystal is increased the stored photonic excitation is spread more and more over shells with higher radius. The spatial

atomic mode then no longer resembles the spatial mode of the probe, which leads to a decrease in efficiency in the writing process. A similar phenomenon then takes place in the reading process, as the atomic spatial excitation profile is no longer optimally matched to the spatial light mode profile.

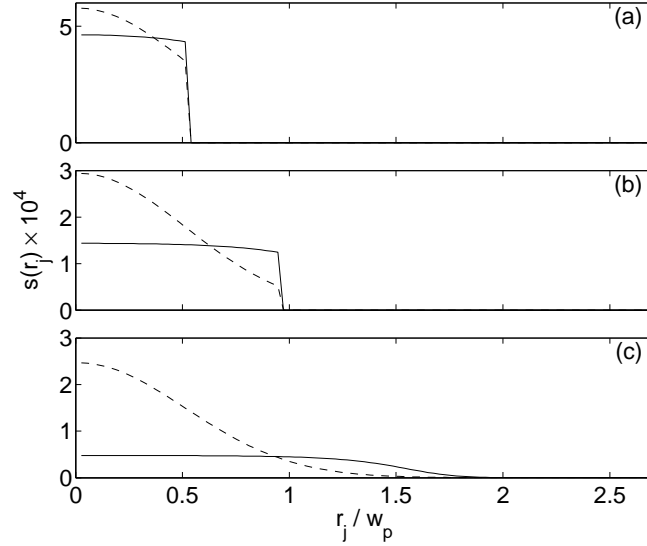


**Figure 4.** Variation of the radial density of excitations after writing in the the extended (dashed) and finite waist (solid) configurations, for different crystal radii [(a)  $R = 0.5w_p$  (b)  $R = 0.95w_p$  (c)  $R = 2.7w_p$ ]. Other parameters as in Fig. 3.

To illustrate this phenomenon, we show in fig. 4 the variation of the radial density of excitations after writing, which is proportional to the surface probability of finding the photonic excitation in the  $j$ -th shell, at the end of the write phase, again in both configurations and for crystals with different radii. The radial density of excitations  $s(r_j)$  is obtained by normalizing the squared modulus of the  $j$ -th shell operator mean value  $S_j(T_w)$  by the number of ions in the shell  $n_j$ ,

$$s(r_j) = |S_j(T_w)|/n_j^2 \quad (29)$$

In the extended configuration, one sees that  $s(r_j)$  reproduces well the spatial Gaussian mode profile of the probe field, as expected from the analytical predictions of sec. 2.3. In the finite waist configuration, the spatial atomic mode defined by  $s(r_j)$  has reasonable overlap with the ideal extended configuration mode (i.e. the probe field mode) for  $R \lesssim w_p$ , but clearly deviates from it as the crystal radius increases and the coupling between the shells causes the excitation to spread more and more radially into the crystal.

To summarize the results and show in particular that the decrease in efficiency for large radii is always substantial in the finite waist configuration, regardless of the length or density of the crystal, fig. 5 shows the variation of the optimized efficiency as a function of the crystal dimensions,  $L$  and  $R$ , for a density of  $6.1 \times 10^8 \text{ cm}^{-3}$ . The range chosen for the dimensions is typical of current experiments with ion Coulomb crystals

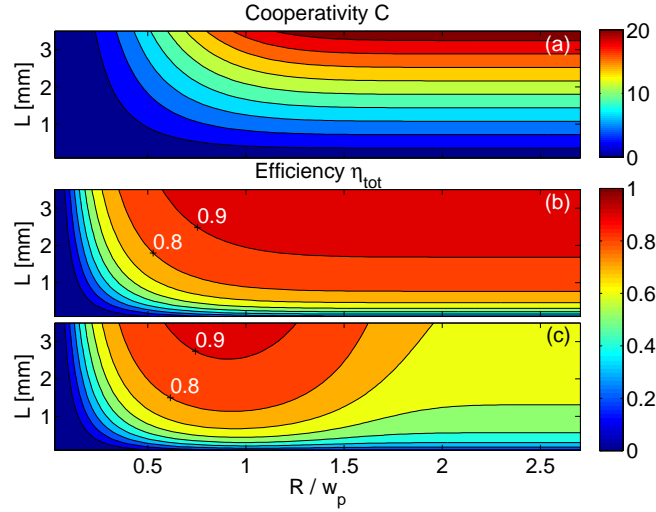


**Figure 5.** (Color online) (a) Variation of the cooperativity as a function of the crystal dimensions  $L$  and  $R$ . (b) Variation of the optimized efficiency in the extended configuration versus  $L$  and  $R$ . (c) Variation of the optimized efficiency in the finite control field waist configuration ( $w_c = w_p$ ) versus  $L$  and  $R$ . The crystal density is  $\rho = 6.1 \times 10^8 \text{ cm}^{-3}$  and the pulse duration  $T = 2 \text{ } \mu\text{s}$ .

in cavity [22, 38]. The optimized quantum memory efficiency in the extended control field configuration is found to agree well with the predictions from the analytical model [eq. 21], and is an increasing function of the crystal length for all radii. This is no longer true in the finite waist configuration for which an optimal radius - of the order of  $w_p$  - exists, for all lengths. However, it can be seen that by choosing the radius of the crystal appropriately to “match” the waist of the cavity mode one can achieve similarly high quantum memory efficiencies ( $> 90\%$ ) as in the extended configuration.

### 3.3. Higher-order modes

In this last section we investigate these spatial mode effects on the storage using higher-order spatial cavity modes. On the one hand, this is motivated by the fact that collective strong coupling with higher-order cavity modes has been demonstrated using ion Coulomb crystals [24], which is promising for multimode (spatial) storage. On the other hand, in view of the previous results, one can wonder how the conclusions drawn for the  $\text{TEM}_{00}$  mode generally hold for higher-order cavity modes, and in particular, if some modes are less sensitive to these spatial effects. A general analysis is beyond the scope of the present paper and we will only focus in this last section on the case of a first-order Laguerre-Gauss cavity mode  $\text{LG}_{01}$ , which preserves the cylindrical symmetry of the problem. We thus assume that the probe field radial modefunction is now given by  $\Psi_p(r) = \sqrt{2}(r/w_p) \exp(-r^2/w_p^2)$ . We then compare the quantum memory efficiency in an extended control field configuration and in a configuration where the control field has the same transverse profile as the probe field ( $\Psi_c(r) = \Psi_p(r)$ ).

Figure 6a shows the variation of the effective number of ions defined by eq. (11) as

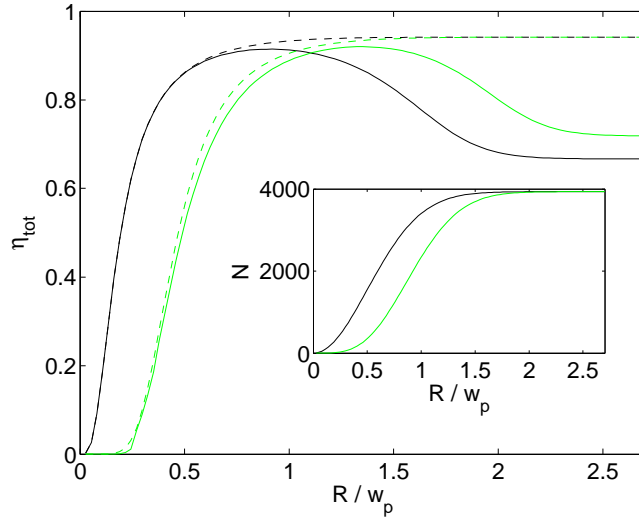


**Figure 6.** (Color online) Variation of the quantum memory efficiency  $\eta_{opt}$  as a function of the crystal radius  $R$ , for the  $\text{TEM}_{00}$  (black) and  $\text{LG}_{01}$  (green) modes and for a crystal with  $L = 3$  mm and  $\rho = 6 \times 10^8 \text{ cm}^{-3}$ . The dashed lines show the extended configuration and the solid lines the finite waist configuration. The inset shows the corresponding variations of the effective number of ions [eq. (11)] as a function of  $R$ , for both modes.

a function of the crystal radius, for a crystal with fixed length and density ( $L = 3$  mm and  $\rho = 6.1 \times 10^8 \text{ cm}^{-3}$ ). As expected,  $N$  increases less rapidly at small radii than for the fundamental mode, on account of the lower coupling at the center of the mode, but saturates at the same value for large radii, because the orthonormal character of the modefunctions. In fig. 6b are represented the corresponding variations of the quantum memory efficiency, both for the  $\text{TEM}_{00}$  and  $\text{LG}_{01}$  modes and in the extended and finite waist configurations. If a similar behavior is qualitatively observed for the  $\text{LG}_{01}$  mode, one can see that the optimal radius is larger for the  $\text{LG}_{01}$  mode ( $R \simeq 1.35w_p$ ) than for the  $\text{TEM}_{00}$  mode ( $R \simeq 0.95w_p$ ). This can be explained by the fact that the regions of high radial intensity for the fields are now located farther away from  $r = 0$ , so that the spreading of the photonic excitations into large radius shells occurs at larger  $R$  and is less pronounced. One can carry out a similar analysis as for the fundamental mode and calculate the variation of the radial density of excitations after writing as a function of the crystal radius. The results are represented in fig. 7 and show the same qualitative conclusions as drawn previously in the case of the fundamental mode.

#### 4. Conclusion

We have investigated the efficiency of a cavity EIT-based quantum memory in which both control and probe fields are coupled to the same cavity mode. Due to the complex spatial atomic mode defined during the EIT process between both fields during the write and read phase of the memory, the optimal efficiency is found to depend not only on the cooperativity parameter, but also the crystal radius. Using parameters from

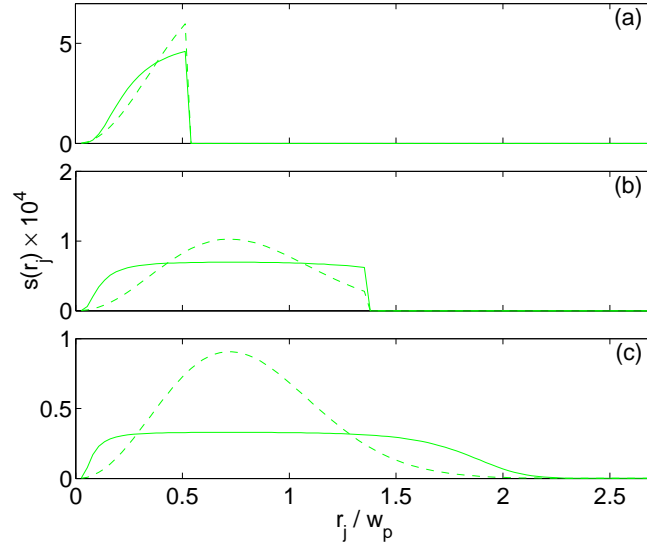


**Figure 7.** (Color online) Variation of the mean surface number of excitations after writing in the the extended (dashed) and finite control field waist (solid) configurations, for different crystal radii [(a)  $R = 0.5w_p$  (b)  $R = 1.35w_p$  (c)  $R = 2.7w_p$ ] and for the LG<sub>01</sub> mode. Other parameters as in Fig. 6.

current experiments with ion Coulomb crystals [22, 25], our simulations predict that high-efficiencies ( $> 90\%$ ) should however be obtainable in this specific configuration.

This theoretical investigation clearly implies that an experimental realization of such an all-cavity EIT quantum memory based on a cylindrical ion Coulomb crystal can be optimized by choosing a crystal with radius matching the waist of the cavity modes. For single species crystals as used in [22, 25], the optimum crystal radius has been found to differ slightly because of the spheroidal (non-cylindrical) shape of such crystals [37], but similar conclusions hold. For two-species crystals, the lighter species typically takes the shape of a nearly perfect cylindrical rod surrounded by the other ion species [37, 38, 39], and matches perfectly the situation considered theoretically. Applying isotope selective photoionization [40], Coulomb crystals consisting of two calcium isotopes can easily be created with varying compositions and shapes [38, 39], providing an ideal situation to test the predictions and optimize the storage conditions.

## Acknowledgments

We acknowledge financial support from the Carlsberg Foundation and the EU via the FP7 projects 'Physics of Ion Coulomb Crystals' (PICC) and 'Circuit and Cavity Quantum Electrodynamics' (CCQED), as well as useful discussions with Ian D. Leroux and Rasmus B. Linnet.

## References

- [1] Duan L M, Lukin M D, Cirac J I and Zoller P 2001 *Nature* **414** 413

- [2] Lukin M D 2003 *Rev. Mod. Phys.* **75** 457
- [3] Kimble H J 2008 *Nature* **453** 1023
- [4] Hammerer K, Sørensen A S and Polzik E S 2010 *Rev. Mod. Phys.* **82** 1041
- [5] Lvovsky A I, Sanders B and Tittel W 2009 *Nature Photon.* **706**
- [6] Simon C *et al.* 2010 *Eur. Phys. J. D* **58** 1
- [7] Chanelière T, Matsukevich D N, Jenkins S D, Lan S-Y, Kennedy T A B and Kuzmich A 2005 *Nature* **438** 833
- [8] Eisaman M D, André A, Massou F, Fleischhauer M, Zibrov A S and Lukin M D 2005 *Nature* **438** 837
- [9] Simon J, Tanji H, Ghosh S and Vuletic V 2007 *Nature Phys.* **3** 765
- [10] Appel J, Figueroa E, Korystov D, Lobino M and Lvovsky A 2008 *Phys. Rev. Lett.* **100** 093602
- [11] Honda K, Akamatsu D, Arikawa M, Yokoi Y, Akiba K, Nagatsuka S, Tanimura T, Furusawa A and Kozuma M 2008 *Phys. Rev. Lett.* **100** 093601
- [12] Cviklinski J, Ortalo J, Laurat J, Bramati A, Pinard M and Giacobino E 2008 *Phys. Rev. Lett.* **101** 133601
- [13] Choi K S, Deng H, Laurat J and Kimble H J 2008 *Nature* **452** 67
- [14] Zhao B, Chen Y-A, Bao X-H, Strassel T, Chu C-S, Jin X-M, Schmiedmayer J, Yuan Z-S, Chen S and Pan J-W 2009 *Nature Phys.* **5** 95
- [15] Zhao R, Dudin Y O, Jenkins S D, Campbell C J, Matsukevich D N, Kennedy T A B and Kuzmich A 2009 *Nature Phys.* **5** 100
- [16] Lukin M D, Yelin S F and Fleischhauer M 200 *Phys. Rev. Lett.* **84** 4232
- [17] Dantan A and Pinard M 2004 *Phys. Rev. A* **69** 043810
- [18] Zimmer F E, André A, Lukin M D and Fleischhauer M 2006 *Opt. Comm.* **264** 441
- [19] Dantan A, Cviklinski J, Pinard M and Grangier P 2006 *Phys. Rev. A* **73** 032338
- [20] Gorshkov A, André A, Lukin M D and Sørensen A S 2007 *Phys. Rev. A* **76** 033804
- [21] Mortensen A, PhD thesis, Aarhus University (2005).
- [22] Herskind P F, Dantan A, Marler J P, Albert M and Drewsen M 2009 *Nature Phys.* **5** 494
- [23] Albert M, Marler J P, Herskind P F, Dantan A and Drewsen M 2012 *Phys. Rev. A* in press (*Preprint* arXiv:1108.0528)
- [24] Dantan A, Albert M, Marler J P, Herskind P F and Drewsen M 2009 *Phys. Rev. A* **80** 041802(R)
- [25] Albert M, Dantan A and Drewsen M 2011 *Nature Photon.* **5** 633
- [26] Dantan A, Albert M and Drewsen M 2012 *Phys. Rev. A* **85** 013840
- [27] Müller G, Müller M, Wicht A, Rinkleff R-H and Danzmann K 1997 *Phys. Rev. A* **56** 2385
- [28] Hernandez G, Zhang J and Zhu Y 2007 *Phys. Rev. A* **65** 053814
- [29] Wu H, Gea-Banacloche J and Xiao M 2008 *Phys. Rev. Lett.* **100** 173602
- [30] Mücke M, Figueroa E, Borchmann J, Hann C, Murr K, Ritter S, Villas-Boas C J and Rempe G 2010 *Nature* **465** 755
- [31] Kampschulte T, Alt W, Brakhane S, Ekstein M, Reimann R, Widera A and Meschede D 2010 *Phys. Rev. Lett.* **105** 155603
- [32] Lauprêtre T, Proux C, Ghosh R, Schwartz S, Goldfarb F and Bretenaker F 2011 *Opt. Lett.* **36** 1551
- [33] Specht H P, Nölleke C, Reiserer A, Uphoff M, Figueroa E, Ritter S and Rempe G 2011 *Nature* **473** 190
- [34] Nagorny B, Elsässer T and Hemmerich A 2003 *Phys. Rev. Lett.* **91** 153003
- [35] Brennecke F, Donner T, Ritter S, Bourdel T, Köhl M and Esslinger T 2007 *Nature* **450** 268
- [36] Colombe Y, Steinmetz T, Dubois G, Linke F, Hunger D and Reichel J 2007 *Nature* **450** 272
- [37] Hornekær L, Kjærgaard N, Thommesen A M and Drewsen M 2001 *Phys. Rev. Lett.* **86** 1994
- [38] Herskind P F, Dantan A, Langkilde-Lauesen M B, Mortensen A, Sørensen J L and Drewsen M 2008 *Appl. Phys. B: Lasers Opt.* **93** 373
- [39] Mortensen A, Nielsen E, Matthey T and Drewsen M 2007 *J. Phys. B: At. Mol. Opt. Phys.* **40**, F223-F229

- [40] Mortensen A, Lindballe J J T, Jensen I S, Staantum P, Voigt D and Drewsen M 2004 Phys. Rev. A **69**, 042502